Korean J. Chem. Eng., 39(6), 1624-1631 (2022)
DOI: 10.1007/s11814-021-1040-9

pISSN: 0256-1115
eISSN: 1975-7220

Performance enhancement of alkaline organic redox flow battery using catalyst including titanium oxide and Ketjenblack

Wonmi Lee*, Gyunho Park*, Daniel Schröder,†, and Yongchai Kwon*,***,****,†**

*Graduate School of Energy and Environment, Seoul National University of Science and Technology, 232 Gongneung-ro, Nowon-gu, Seoul 01811, Korea
**Institute of Energy and Process Systems Engineering (InES), Technische Universität Braunschweig, Langer Kamp 19b, 38106 Braunschweig, Germany
***Department of Chemical and Biomolecular Engineering, Seoul National University of Science and Technology, 232 Gongneung-ro, Nowon-gu, Seoul 01811, Korea
****Department of New and Renewable Energy Convergence, Seoul National University of Science and Technology, 232, Gongneung-ro, Nowon-gu, Seoul 01811, Korea
(*Received 7 October 2021 • Revised 2 December 2021 • Accepted 13 December 2021*)

Abstract−Carbon felt (CF) doped by catalyst including titanium oxide and ketjen black (TiO_2/KB-CF) is used as negative electrode to enhance the redox reactivity of napthoquinone (NQSO) and thus the performance of aqueous organic redox flow batteries (AORFBs). The redox reactivity of NQSO is better with TiO_2/KB-CF than with pristine CF (anodic current density of 13.3 and 19.8 $mA \cdot cm^{-2}$, and cathodic current density of −15.7 and −21.9 $mA \cdot cm^{-2}$ with pristine CF and TiO_2/KB-CF), while the reaction reversibility of NQSO is also enhanced in TiO_2/KB-CF (ratio of peak current density is 0.84 and 0.9 with pristine CF and TiO_2/KB-CF). These results are due to the hydrophilic and conductive properties of the TiO_2/KB catalyst. TiO_2 can hold many hydroxyl groups that are hydrophilic and electro-active group, while KB is a conductive material that induces a fast electron transfer. With these benefits, the charge transfer resistance of the electrode is reduced from 1.8 Ω with pristine CF to 1.5 Ω with TiO_2/KB-CF. In AORFB tests using NQSO and potassium ferrocyanide under alkaline supporting electrolyte, energy efficiency increased from 58% (pristine CF) to 61% (TiO_2/KB-CF) with a low capacity loss rate of 0.006 $Ah \cdot L^{-1}$ per cycle and the cross-over rate of active materials during cycling of AORFB was very low.

Keywords: Alkaline Organic Redox Flow Battery, Titanium Oxide, Ketjen Black, Catalyst Effect, Naphthoquinone Derivatives

INTRODUCTION

Energy storage systems (ESSs) are important for renewable energy to be used effectively; examples of ESSs are fuel cells, capacitors, lithium ion batteries and redox flow batteries [1-13].

Among the various types of ESSs, the redox flow battery (RFB) has a variety of advantages especially for large-scale applications because the power and energy can be scaled separately from each other by stack and tank, respectively [14-19]. There are three main factors that can determine the power and energy in RFBs: cell voltage, ionic conductivity, and the number of electrons involved in the redox reaction [14]. These factors are predominantly affected by the active materials and electrolytes, electrodes, and membrane [15]. Supporting electrolytes of the RFBs are divided into non-aqueous RFB and aqueous RFB. The non-aqueous RFB can provide a high cell voltage because no hydrogen or oxygen evolution occurs in the electrolyte [16]. However, the ionic conductivity of non-aqueous electrolyte is far lower than that of aqueous electrolyte [17]. Therefore, recently, it has been known that aqueous RFB may be better suited to provide high power and energy density [18]. In addition, this is safer than non-aqueous RFB because of the non-volatile property of supporting electrolyte and active materials in the aqueous RFB [19].

Among aqueous RFB systems, vanadium redox flow battery (VRFB) has been developed and utilized as commercial applications due to its high performance [20-36]. VRFBs have various advantages. First, vanadium ions can be used as active materials in both electrolytes [20-27]. The use of the same active material in both electrolytes can lead to less cross-over through the membrane, which induces a better stability than for other metal-based RFB systems, such as Fe-Cr RFB or Zn-Br RFB. Second, its cell voltage is 1.26 V, which is a relatively high value among aqueous RFB systems [20, 21]. Therefore, this can lead to high power and energy density. Third, the solubility of vanadium ions in sulfuric acid is high (~1.8 M), and this results in a high energy density [22,23]. However, the VRFB system has some obvious limitations: First, vanadium is very expensive because it is a rare-earth metal and, thus, the amount that can be excavated is limited [24,25]. Second, there is still cross-over from electrode to electrode of vanadium ions because of their small size, and this may induce a rapid capacity decay during cycling. To alleviate the issue, an additional re-balancing process is required [26, 27]. Third, the temperature window is narrow due to precipitation

†To whom correspondence should be addressed.
E-mail: d.schroeder@tu-braunschweig.de, kwony@seoultech.ac.kr

of vanadium ions above 45 °C or below 0 °C [28,29]. This implies that VRFB can be operated in only a limited environment. Fourth, additional catalyst has to be doped on the electrode to improve the redox reactivity of vanadium ions, and this leads to a higher cost of the RFB system [30-36].

To solve the problems of VRFBs, organic materials can be considered as active materials to replace vanadium. Aqueous organic redox flow batteries (AORFB) using organic molecules as redox active materials have many merits compared to conventional VRFB [37-41]. First, the temperature range of organic materials is wide because the organic materials do not induce the precipitation issue, especially at high temperature [37,38]. Second, their projected cost is much cheaper than vanadium because they can be obtained by natural sources and further synthesized on a large scale [39]. Third, the capacity of AORFBs can be twice as much as that of VRFBs when the same concentrations of active materials are used [40]. This is because the number of electrons involved in the redox reaction of organic materials such as quinones is two, whereas that of vanadium is only one. Fourth, the redox reactivity of organic materials is high and, thus, it is less required to use catalysts [41].

Candidates as active material for AORFB are, among others, quinones, aza-aromatics, methyl viologens as well as TEMPO derivatives [37-41]. Among them, quinones have been used widely because they can be utilized in a wide range of supporting electrolyte pHs, depending on the functional groups doped on the quinone molecules [42-48] as well as for modifying its base structure [49]. For example, quinones containing sulfonate groups are used in acidic pHs such as sulfuric acid [50-52]. More specifically, anthraquinone-2,6-disulfonic acid and 4,5-dihydroxy-1,3-benzenedisulfonic acid were introduced and developed in sulfuric acid [50].

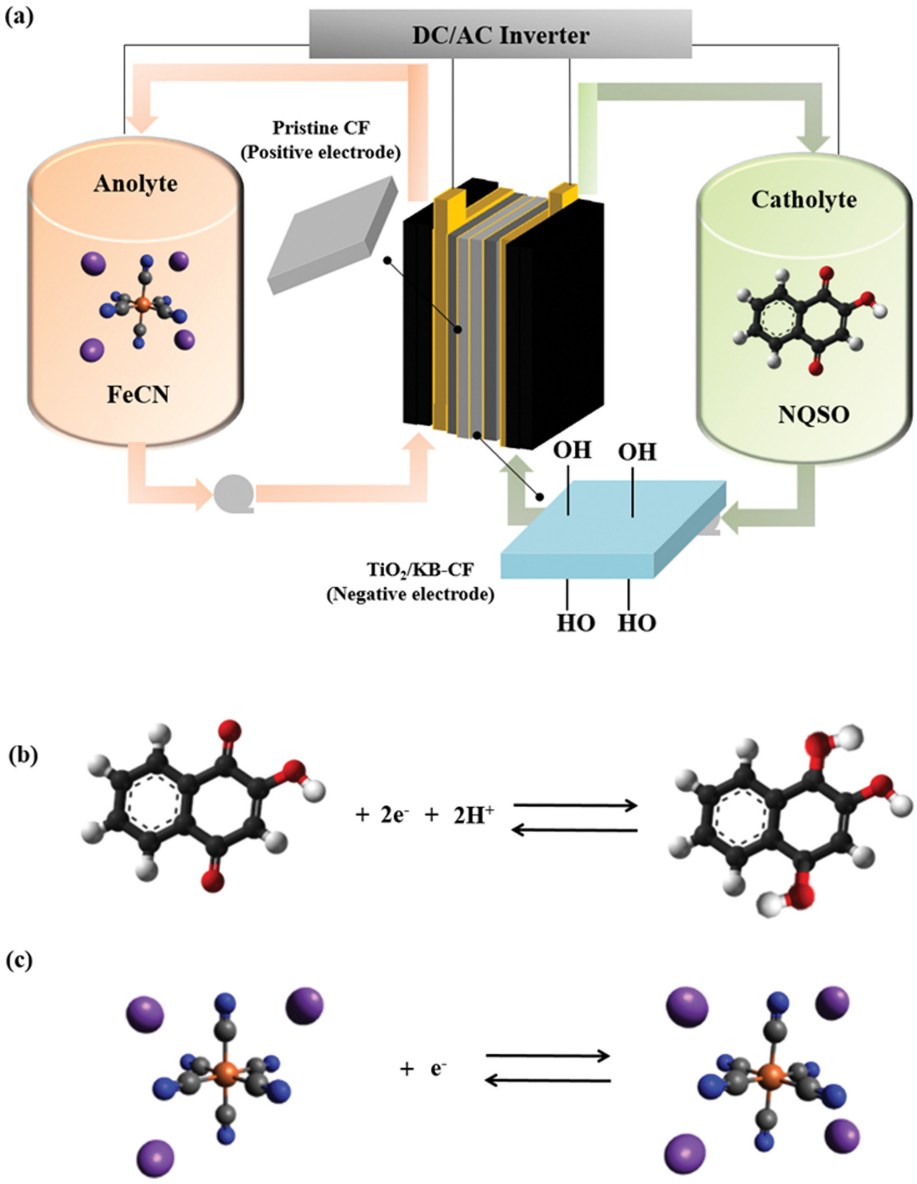

Fig. 1. A schematic of (a) AORFB full cell structure using TiO_2/KB-CF as negative electrode and the redox reactions of (b) NQSO and (c) FeCN dissolved in alkaline electrolyte.

However, a nucleophilic attack formed an undesirable side reaction and transformation of 4,5-dihydroxy-1,3-benzendisulfonic acid. Therefore, a new benzoquinone derivative was proposed and the transformation process was optimized [51-53]. As another example, quinones containing hydroxyl groups were used as active materials in alkaline supporting electrolyte pHs [54-56]. More specifically, dihydroxy anthraquinone and ferrocyanide were used as active materials in potassium hydroxide [54]. Their cell voltage was 1.2 V and the efficiency of AORFB using them was good. However, the side reaction of anthraquinone derivatives induced the capacity fade of AORFB slightly. To overcome the bottleneck, chemically stable anthraquinone derivatives were synthesized and optimized by computational [55] and experimental methods. As a result, the stability of AORFBs using anthraquinone derivatives was improved [56]. Besides the anthraquinone derivatives, naphthoquinone derivatives were utilized [57]. Lastly, some quinones with hydrophilic groups were used as active materials for neutral or near-neutral supporting electrolyte pHs, and special additives were developed to enhance the solubility of quinone derivatives in aqueous media [58-61].

In this study, mixed naphthoquinone derivatives (NQSO) and potassium ferrocyanide (FeCN) were used as negative and positive active materials, while both were dissolved in 1 M KOH [57]. To improve the redox properties of NQSO that can be dimerized during cycling of AORFB at high concentration conditions, a catalyst including titanium (IV) oxide/ketjen black (TiO_2/KB) was introduced. The TiO_2/KB was then doped onto the surface of carbon felt (TiO_2/KB-CF) for use as negative electrode. Here, TiO_2 has abundant oxygen functional groups that can improve the redox reactivity of active materials for RFB [62], and KB combined with conductive carbon materials can enhance the conductivity [63]. Thus, TiO_2 and KB can be used together to enhance the redox properties of NQSO. With that, the electrochemical performance of TiO_2/KB-CF was investigated to examine whether the TiO_2/KB-CF promoted the enhancement in the redox properties of NQSO, which can increase the efficiency of AORFB.

A schematic of AORFB full cell structure using the modified electrode, and the redox reactions of NQSO and FeCN dissolved in KOH are shown in Fig. 1.

EXPERIMENTAL

1. Materials

Catholyte consists of supporting electrolyte and negative active material, while anolyte consists of supporting electrolyte and positive active material, and they are the main components of AORFB. To prepare the catholyte and anolyte consisting of NQSO and FeCN, naphthoquinone-4-sulfonic acid sodium salt and 2-hydroxy naphthoquinone were purchased from Alfa Aesar. Potassium hexacyanoferrate(II) trihydrate was from Sigma Aldrich. Potassium hydroxide (95.0%) that was used for supporting electrolyte solution was obtained from Samchun Chemical. For fabricating the catalyst solution, ketjen black, TiO_2 powder and ethanol were obtained from Samchun Chemical and Nafion 117 solution was purchased from Sigma Aldrich. In addition, the Nafion membrane (Nafion 117 (N117)) was from the Sigma Aldrich and put in de-ionized (DI) water for 24 h before use.

2. Electrochemical Measurements

2-1. Electrochemical Characterization

To investigate the effect of temperature on the electrochemical properties of NQSO and ferrocyanide, cyclic voltammograms (CVs) were measured. Pt wire and Ag/AgCl were used as counter and reference electrodes, respectively, and glass carbon electrode (GCE, 5 mm diameter, active area 0.196 cm^2) was considered as working electrode. The scan rate used was 100 $mV \cdot s^{-1}$. As electrolytes, 0.01 M

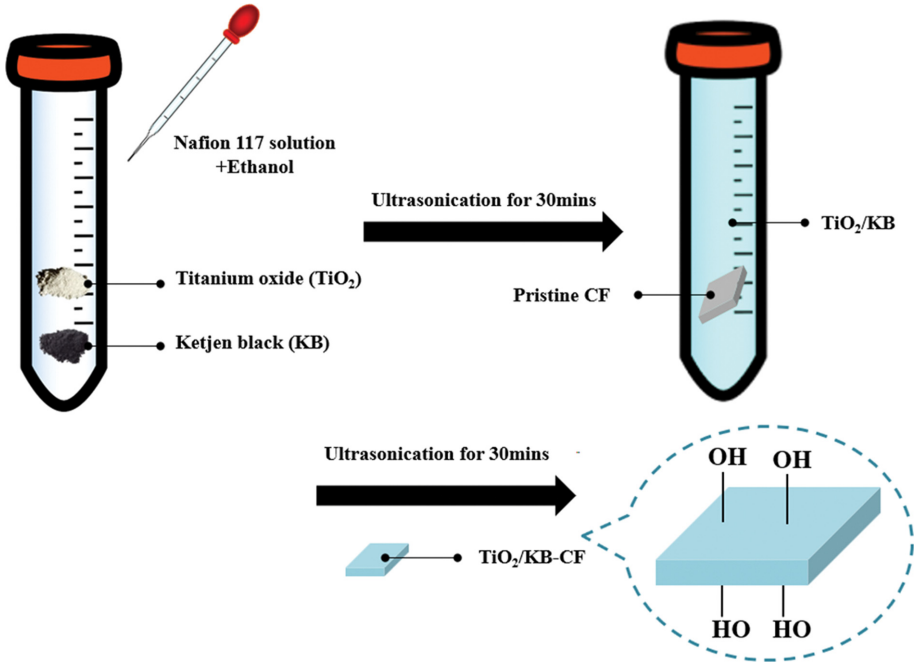

Fig. 2. The synthetic procedure of TiO_2/KB-CF electrode.

of both NQSO and ferrocyanide was dissolved into 20 mL of 1.0 M KOH solution.

To compare the redox properties at various concentrations of NQSO, 0.0002 mol and 0.002 mol of NQSO were dissolved into 20 mL of 1.0 M KOH solution, and their CV curves were measured. In addition, to synthesize the TiO_2/KB catalyst ink, Ketjen black, TiO_2 powder, Nafion 117 solution, and ethanol were mixed by using ultrasonic blending for 1 h to disperse the materials uniformly [64]. Carbon felt (CF) and the catalyst ink doped carbon felt (TiO_2/KB-CF) were used as working electrode.

The samples before and after AORFB full cell testing were collected and CV curves were measured with the samples to investigate how the active materials crossed over through the membrane during cycling.

2-2. Performance Evaluation of AORFB Full Cells

For AORFB full cell tests, charge-discharge equipment (Wonatech, WBCS3000) was used. As catholyte, 0.006 mol NQSO was dissolved in 1.0 M KOH solution, and 20 mL of such prepared catholyte was filled with tank, while 0.015 mol ferrocyanide was dissolved in 1.0 M KOH solution as anolyte, and 50 mL of the anolyte was filled with tank. The higher amount of ferrocyanide was used to fix the redox reaction of anolyte as a rate determining step. Carbon felt (CF) (SGL 4.6 GFD, active area of 4 cm^2 and thickness of 4.7 mm) was used as electrode. During charge and discharge cycling of the AORFB, 100 $mA \cdot cm^{-2}$ was applied under the cut-off voltage ranges of 0.2-1.6 V and the flow rate of 25 $mL \cdot min^{-1}$.

To investigate the effect of TiO_2/KB catalyst on the performance of AORFB using NQSO and ferrocyanide, TiO_2/KB catalyst ink was prepared and doped onto CF (TiO_2/KB-CF). To bind the TiO_2/KB catalyst on CF, Nafion 117 solution was used as binder. After mixing them, ultrasonication was performed, and with this process TiO_2/KB-CF was well formed. Fig. 2 shows the synthetic procedure of TiO_2/KB-CF electrode. This TiO_2/KB-CF was used as negative electrode for AORFB full cell tests. In addition, all membranes were pre-treated in DI water for 24 h before use.

RESULTS AND DISCUSSION

1. The Effect of Concentration of NQSO on the Redox Reactivity of NQSO

To evaluate the impact of the concentration of NQSO on the redox reactivity of NQSO, a low concentration (0.01 M) and a high concentration (0.1 M) of NQSO dissolved in 1 M KOH were evaluated by CV. As shown in Fig. 3, the peak separation between anodic and cathodic potentials of NQSO at low concentration (0.01 M) was 0.08 V, while that of NQSO at high concentration (0.1 M) was 0.13 V. This result means that the electron transfer rate of NQSO at high concentration is slower than that at low concentration. A possible reason for this result is the dimerization of NQSO molecules occurring at their high concentration ranges [65]. This dimerization can be facilitated during cycling of AORFB because a large amount of the NQSO molecules that are reduced and oxidized agglomerate together during cycling, and this increases their viscosity and decreases the voltage efficiency (VE) of AORFB. To alleviate this issue of NQSO, the adoption of advanced electrode can be considered.

2. The Effect of TiO_2/KB Catalyst on the Electrochemical Properties of NQSO

To further enhance the redox property of NQSO, the TiO_2/KB catalyst was prepared via ultrasonication method. Here, Ketjen black (KB), which is a conductive material, can facilitate the electron transfer rate, and it was then mixed with TiO_2 [66]. TiO_2 has many hydroxyl groups that are hydrophilic, and the oxygen-containing groups belonging to TiO_2 are electroactive. Both properties can

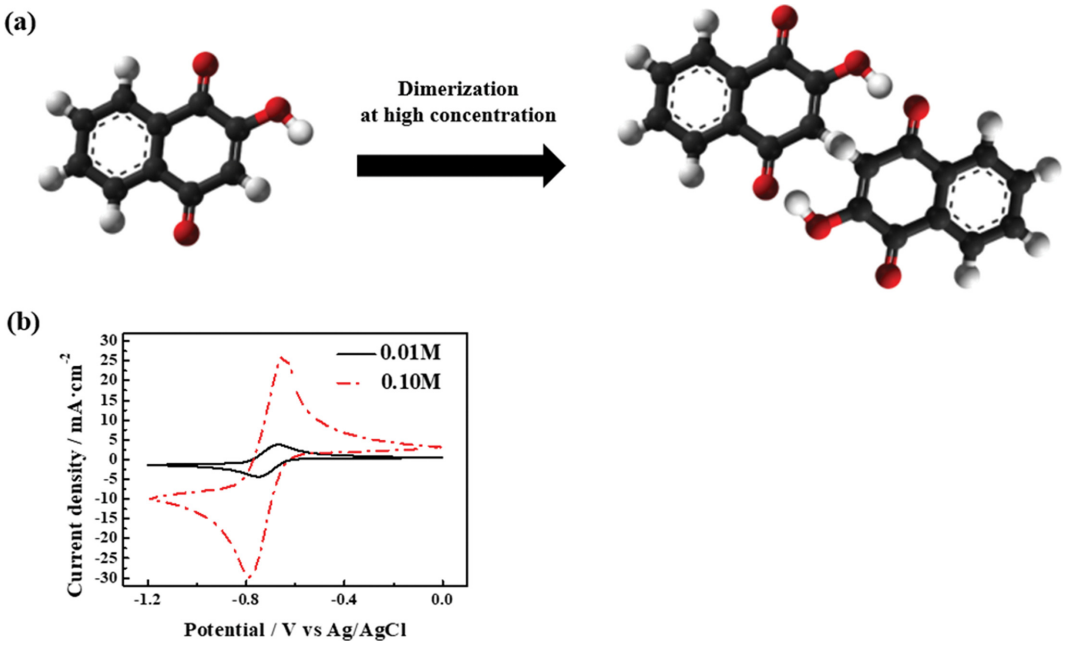

Fig. 3. (a) Dimerization process of NQSO molecules occurring at their high concentration ranges, and (b) CV curves representing the redox properties of NQSO measured in the two different concentrations (0.01 and 0.10 M) with a scan rate of 100 mV s^{-1}.

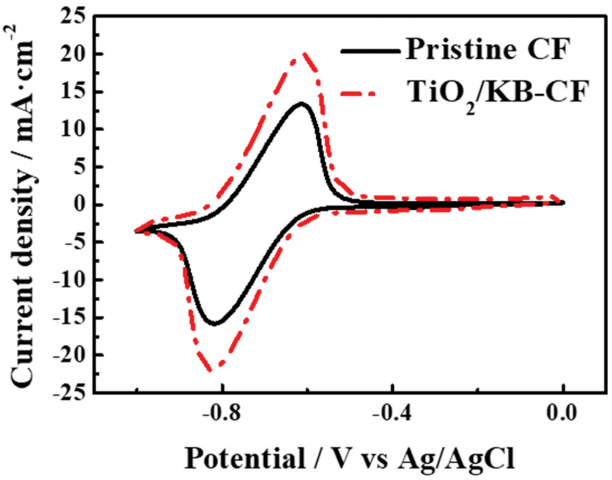

Fig. 4. CV curves of NQSO dissolved in KOH that are measured in both pristine CF and TiO_2/KB-CF.

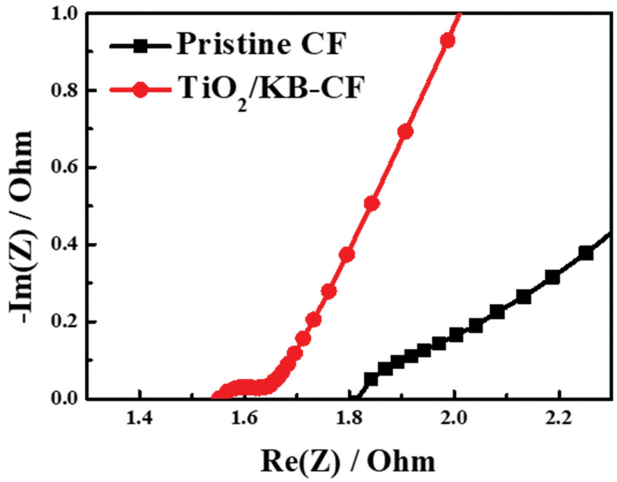

Fig. 5. Nyquist plots of NQSO dissolved in 1.0 M KOH solution measured with the use of pristine CF and TiO_2/KB-CF.

increase the redox reactivity of the electrode in combination with the active material [67].

To evaluate the impact of the TiO_2/KB catalyst on the electrochemical properties of NQSO, CV curves and impedance spectroscopy measurements of NQSO dissolved in KOH were performed in both pristine CF and TiO_2/KB-CF (Figs. 4 and 5). According to Fig. 4, the redox reactivity and reversibility of NQSO were enhanced with the use of TiO_2/KB catalyst. More specifically, in terms of the redox reactivity of NQSO, its oxidation current peak was more improved with TiO_2/KB-CF than with pristine CF. Next, in terms of reversibility of NQSO redox reaction, the ratio of anodic to cathodic peaks was improved from 0.84 (pristine CF) to 0.90 (TiO_2/KB-CF). This indicates that the redox reaction of NQSO becomes faster with the use of TiO_2/KB catalyst, and this is because of the unique benefits of TiO_2/KB catalyst, which are electroactive property, abundant hydrophilic groups and excellent conductivity [66,67].

The above result is confirmed by the Nyquist plots using EIS of NQSO measured in both pristine CF and TiO_2/KB-CF (Fig. 5). The charge transfer resistance of NQSO was reduced from 1.8 Ω (pristine CF) to 1.5 Ω (TiO_2/KB-CF). This finding indicates that when TiO_2/KB-CF is used, the charge transfer resistance of NQSO is reduced and its electron transfer rate increases [66,67].

3. The Effect of TiO_2/KB-CF Electrode on the Performance of AORFBs using NQSO and FeCN

To identify the impact of the TiO_2/KB catalyst on the performance of AORFBs using NQSO and FeCN as redox couple in alkaline pH supporting electrolytes, AORFB full cell tests using pristine CF and TiO_2/KB-CF as negative electrode were implemented. Here, the other conditions for operating AORFB full cells (except the negative electrode) were the same, which means that only TiO_2/KB catalyst doped on CF can affect the performance of AORFBs. The charge-discharge curves and discharging capacity pattern are shown in Fig. 6. There are two advantages that can be seen in Fig. 6(a). First, when TiO_2/KB-CF was used, the over-potential of for the reaction of NQSO was reduced, while this was well matched with that obtained from half-cell results. Namely, with the use of TiO_2/KB-CF, the electron transfer rate of NQSO that contacted the TiO_2/KB-CF electrode was improved, while its resistance and over-potential were reduced [68]. Second, the capacity of the AORFB full cell using TiO_2/KB-CF increased. The average discharging capacity was enhanced from 10.6 $Ah{\cdot}L^{-1}$ (pristine CF) to 11.5 $Ah{\cdot}L^{-1}$ (TiO_2/KB-CF). Regarding capacity retention rate as shown in Fig. 6(b),

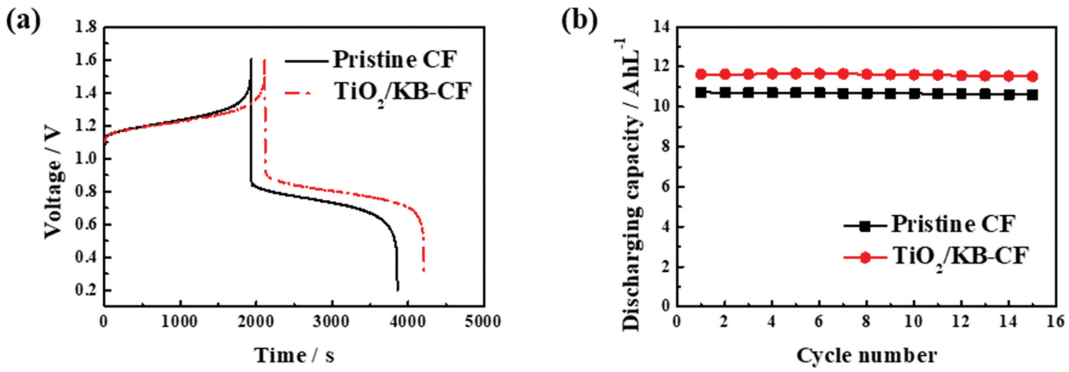

Fig. 6. (a) Charge-discharge curve of AORFBs using NQSO and ferrocyanide as redox couple measured at 10th cycle and (b) their discharging capacities measured during cycling of AORFB. Here, as negative electrode, pristine CF and TiO_2/KB-CF were used, while the applied current density was 100 $mA{\cdot}cm^{-2}$.

this was the same irrespective of the use of catalyst. More specifically, the capacity loss rate of both AORFBs was 0.006 $Ah \cdot L^{-1}$ per cycle for 15 cycles (the capacity loss rate of 0.062% per cycle) during 15 cycles). This means that the TiO_2/KB catalyst plays an important role in increasing the capacity of AORFB full cell with the reduced overpotential of NQSO without a meaningful sacrifice in the cycling stability of AORFB.

The effect of TiO_2/KB catalyst on the efficiency of AORFBs using NQSO and ferrocyanide is represented in Fig. 7. According to Fig. 7, CE of the two AORFBs was almost same as 99% during cycling of AORFB irrespective of the use of catalyst. This means that the size of NQSO and ferrocyanide that is included in electrolytes is large enough, and it is difficult for these molecules to permeate through the membrane. However, different from CE, VE was significantly affected by the type of electrode. Quantitatively, that of AORFBs was improved from 59% (pristine CF) to 62% (TiO_2/KB-CF). This result can be explained that the excellent attributes of TiO_2/KB-CF promote redox reactivity, reversibility, and electron transfer rate of NQSO molecules whose redox reaction is a rate determining step. More specifically, the abundant hydroxyl groups included in TiO_2 of TiO_2/KB catalyst can lead to faster redox reactivity of NQSO molecules, and the excellent conductivity included in KB of TiO_2/KB can also affect the increase in electron transfer rate of NQSO molecules [66,67]. Accordingly, EE of AORFBs measured at high current density of 100 $mA \cdot cm^{-2}$ was also improved from 58% (pristine CF) to 61% (TiO_2/KB-CF).

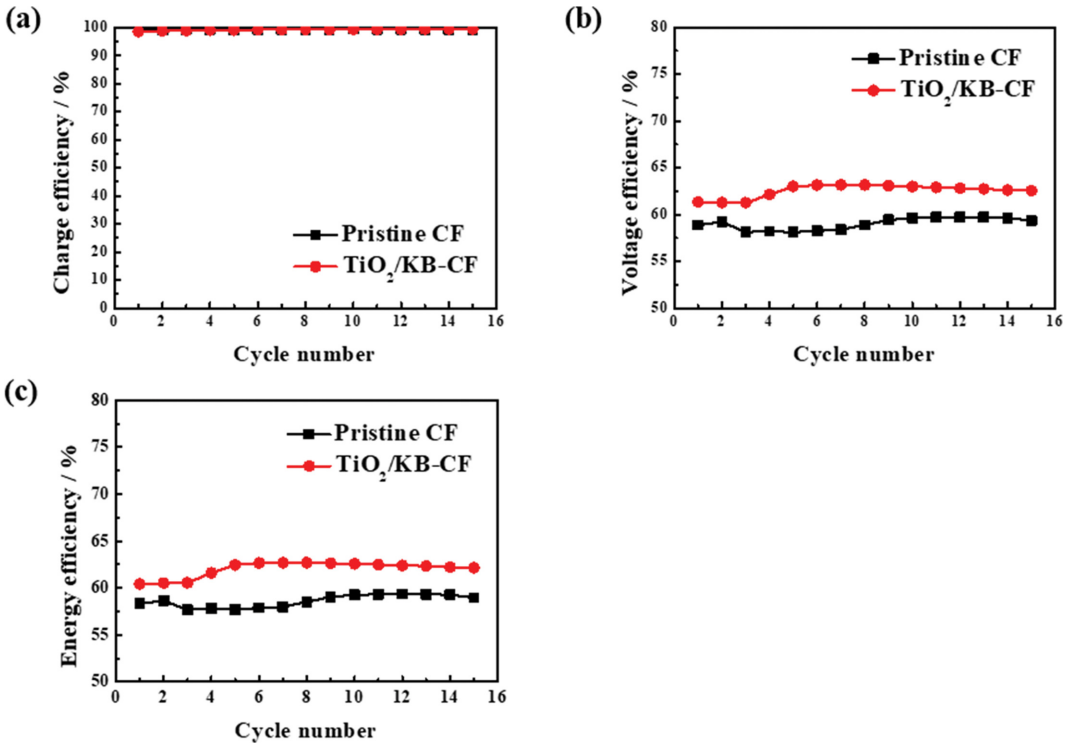

Fig. 7. (a) Charge efficiency, (b) voltage efficiency and (c) energy efficiency graphs measured during cycling of AORFBs using NQSO and ferrocyanide as redox couple. Here, as negative electrode, pristine CF and TiO_2/KB-CF were used, while the applied current density was 100 $mA \cdot cm^{-2}$.

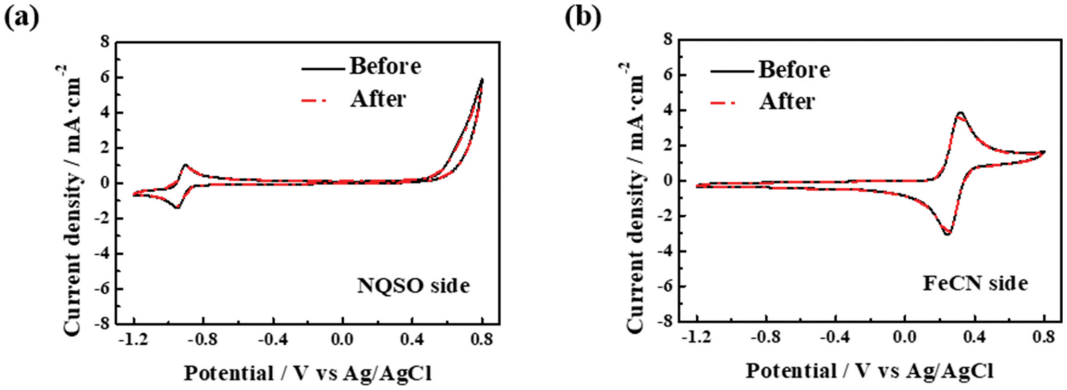

Fig. 8. CV curves of (a) NQSO and (b) FeCN solutions measured before and after AORFB full cell test using TiO_2/KB-CF as negative electrode.

To evaluate the crossover of active materials through the membrane occurring during cycling of AORFBs using NQSO and FeCN as the active materials, CV curves of NQSO and FeCN solutions before and after AORFB full cell tests using TiO_2/KB-CF as negative electrode are measured (Fig. 8). As mentioned, due to the large size of active materials and the Nafion membrane with high selectivity, the crossover of active materials can almost be excluded during the AORFB full cell test.

CONCLUSION

TiO_2/KB-CF was considered as negative electrode to improve the redox reactivity of NQSO and the performance of AORFB using the NQSO as active material. The redox reactivity of NQSO was better in TiO_2/KB-CF than in CF. In addition, the reaction reversibility of NQSO was enhanced with the use of TiO_2/KB-CF (ratio of peak current density was 0.84 and 0.9 with CF and TiO_2/KB-CF). These results are due to the hydrophilic and conductive properties of TiO_2/KB catalyst included in TiO_2/KB-CF electrode. Here, TiO_2 played a role in keeping as many as possible hydroxyl groups that were hydrophilic and electro-active group, and KB was a conductive material facilitating a fast electron transfer. With these, the charge transfer resistance of electrode was reduced to 1.5 Ω with TiO_2/KB-CF. Based on that, in AORFB tests using NQSO and FeCN as redox couple under alkaline supporting electrolyte, its EE increased to 61% with the use of TiO_2/KB-CF, while its capacity loss rate was low as 0.006 $Ah \cdot L^{-1}$ per cycle and no cross-over of active materials was observed during cycling of AORFB.

ACKNOWLEDGEMENT

This study was supported by the Research Program funded by the SeoulTech (Seoul National University of Science and Technology).

REFERENCES

1. H. Niaz, M. MansourLakouraj and J. Liu, *Korean J. Chem. Eng.*, **38**, 1617 (2021).
2. D. Yadav, S. Kumar, O. P. Verma, N. Pachauri and V. Sharma, *Korean J. Chem. Eng.*, **38**, 906 (2021).
3. M. R. Karim, T. H. Han, S. Y. Sawant, J. J. Shim, M. Y. Lee, W. K. Kim, J. S. Kim and M. H. Cho, *Korean J. Chem. Eng.*, **37**, 1241 (2020).
4. J. S. Seo and B. K. Na, *Korean J. Chem. Eng.*, **38**, 1826 (2021).
5. G. Kear, A. A. Shah and F. C. Walsh, *Int. J. Energy Res.*, **36**, 1105 (2012).
6. A. Nulu, V. Nulu, J. S. Moon and K. Y. Sohn, *Korean J. Chem. Eng.*, **38**, 1923 (2021).
7. E. H. Lim, J. Y. Chun, C. S. Jo and J. K. Hwang, *Korean J. Chem. Eng.*, **38**, 227 (2021).
8. M. Hwang, J. S. Jeong, J. C. Lee, S. I. Yu, H. S. Jung, B. S. Cho and K. Y. Kim, *Korean J. Chem. Eng.*, **38**, 454 (2021).
9. L. Fan, P. Sun, L. Yang, Z. Xu and J. Han, *Korean J. Chem. Eng.*, **37**, 166 (2020).
10. J. H. Kim, S. I. Mo, G. S. Park and J. W. Yun, *Korean J. Chem. Eng.*, **38**, 1834 (2021).
11. R. Bahoosh, M. Jafari and S. S. Bahrainian, *Korean J. Chem. Eng.*, **38**, 1703 (2021).
12. L. Li, S. Kim, W. Wang, M. Vijayakumar, Z. Nie, B. Chen, J. Zhang, G. Xia, J. Hu, G. Graff, J. Liu and Z. Yang, *Adv. Energy Mater.*, **1**, 394 (2011).
13. M. Christwardana, Y. Chung and Y. Kwon, *Korean J. Chem. Eng.*, **34**, 3009 (2017).
14. A. Z. Weber, M. M. Mench, J. P. Meyers, P. N. Ross, J. T. Gostick and Q. Liu, *J. Appl. Electrochem.*, **41**, 1137 (2011).
15. J. Noack, N. Roznyatovskaya, T. Herr and P. Fischer, *Angew. Chem. Int. Ed.*, **54**, 9776 (2015).
16. P. Alotto, M. Guarnieri and F. Moro, *Renew. Sustain. Energy Rev.*, **29**, 325 (2014).
17. S. H. Shin, S. H. Yun and S. H. Moon, *RSC Adv.*, **3**, 9095 (2013).
18. Q. Liu, A. E. Sleightholme, A. A. Shinkle, Y. Li and L. T. Thompson, *Electrochem. Commun.*, **11**, 2312 (2009).
19. W. Lee, B. W. Kwon, M. Jung, D. Serhiichuk, D. Henkensmeier and Y. Kwon, *J. Power Sources*, **439**, 227079 (2019).
20. H. T. T. Pham, C. Jo, J. Lee and Y. Kwon, *RSC Adv.*, **6**, 17574 (2016).
21. C. Noh, S. Moon, Y. Chung and Y. Kwon, *J. Mater. Chem. A*, **5**, 21334 (2017).
22. C. Noh, C. S. Lee, W. S. Chi, Y. Chung, J. H. Kim and Y. Kwon, *J. Electrochem. Soc.*, **165**, A1388 (2018).
23. R. A. Elgammal, Z. Tang, C. N. Sun, J. Lawton and T. A. Zawodzinski Jr., *Electrochim. Acta*, **237**, 1 (2017).
24. H.-Y. Jung, M.-S. Cho, T. Sadhasivam, J.-Y. Kim, S.-H. Roh and Y. Kwon, *Solid State Ion.*, **324**, 69 (2018).
25. S. Jeong, L. H. Kim, Y. Kwon and S. Kim, *Korean J. Chem. Eng.*, **31**, 2081 (2014).
26. C. N. Sun, Z. Tang, C. Belcher, T. A. Zawodzinski and C. Fujimoto, *Electrochem. Commun.*, **43**, 63 (2014).
27. C. Noh, M. Jung, D. Henkensmeier, S. W. Nam and Y. Kwon, *ACS Appl. Mater. Interfaces*, **9**, 36799 (2017).
28. B. Schwenzer, J. Zhang, S. Kim, L. Li, J. Liu and Z. Yang, *ChemSusChem*, **4**, 1388 (2011).
29. C. Choi, S. Kim, R. Kim, Y. Choi, S. Kim, H. Y. Jung, J. H. Yang and H. T. Kim, *Renew. Sustain. Energy Rev.*, **69**, 263 (2017).
30. L. Wei, T. S. Zhao, L. Zeng, Y. K. Zeng and H. R. Jiang, *J. Power Sources*, **341**, 318 (2017).
31. A. Di Blasi, C. Busaccaa, O. Di Blasia, N. Briguglioa, G. Squadritoa and V. Antonuccia, *Appl. Energy*, **190**, 165 (2017).
32. Z. González, A. Sánchez, C. Blanco, M. Granda, R. Menéndez and R. Santamaría, *Electrochem. Commun.*, **13**, 1379 (2011).
33. M. Vijayakumar, L. Li, G. Graff, J. Liu, H. Zhang, Z. Yang and J. Z. Hu, *J. Power Sources*, **196**, 3669 (2011).
34. Y. Chung, C. Noh and Y. Kwon, *J. Power Sources*, **438**, 227063 (2019).
35. C. Noh, B. W. Kwon, Y. Chung and Y. Kwon, *J. Power Sources*, **406**, 26 (2018).
36. W. Lee, C. Jo, S. Youk, H. Y. Shin, J. Lee, Y. Chung and Y. Kwon, *Appl. Surf. Sci.*, **429**, 187 (2018).
37. W. Lee, G. Park, D. Chang and Y. Kwon, *Korean J. Chem. Eng.*, **37**, 2326 (2020).
38. C. Chu, B. W. Kwon, W. Lee and Y. Kwon, *Korean J. Chem. Eng.*, **36**, 1732 (2019).
39. C. DeBruler, B. Hu, J. Moss, J. Luo and T. L. Liu, *ACS Energy Lett.*,

3, 663 (2018).
40. J. Winsberg, C. Stolze, S. Muench, F. Liedl, M. D. Hager and U. S. Schubert, *ACS Energy Lett.*, **1**, 976 (2016).
41. J. Winsberg, T. Hagemann, T. Janoschka, M. D. Hager and U. S. Schubert, *Angew. Chem. Int. Ed.*, **56**, 686 (2017).
42. W. Lee, G. Park, Y. Kim, D. Chang and Y. Kwon, Y., *Chem. Eng. J.*, **398**, 125610 (2020).
43. X. Wei, W. Pan, W. Duan, A. Hollas, Z. Yang, B. Li, Z. Nie, J. Liu, D. Reed, W. Wang and V. Sprenkle, *ACS Energy Lett.*, **2**, 2187 (2017).
44. W. Lee, B. W. Kwon and Y. Kwon, *ACS Appl. Mater. Interfaces*, **10**, 36882 (2018).
45. K. Lin, R. Gómez-Bombarelli, E. S. Beh, L. Tong, Q. Chen, A. Valle, A. Aspuru-Guzik, M. J. Aziz and R. G. Gordon, *Nat. Energy*, **1**, 1 (2016).
46. W. Lee and Y. Kwon, *Korean Chem. Eng. Res.*, **57**, 695 (2019).
47. T. Liu, Z. Wei, Z. Nie, V. Sprenkle and W. Wang, *Adv. Energy Mater.*, **6**, 1501449 (2016).
48. G. Park, W. Lee and Y. Kwon, *Korean Chem. Eng. Res.*, **57**, 868 (2019).
49. J. D. Hofmann, F. L. Pfanschilling, N. Krawczyk, P. Geigle, L. Hong, S. Schmalisch, H. A. Wegner, D. Moleenhauer, J. Janek and D. Schröder, *Chem. Mater.*, **30**, 762 (2018).
50. B. Yang, L. Hoober-Burkhardt, F. Wang, G. S. Prakash and S. R. Narayanan, *J. Electrochem. Soc.*, **161**, A1371 (2014).
51. L. Hoober-Burkhardt, S. Krishnamoorthy, B. Yang, A. Murali, A. Nirmalchandar, G. S. Prakash and S. R. Narayanan, *J. Electrochem. Soc.*, **164**, A600 (2017).
52. A. Permatasari, W. Lee and Y. Kwon, *Chem. Eng. J.*, **383**, 123085 (2020).
53. J. D. Hofmann, S. Schmalisch, S. Schwan, L. Hong, H. A. Wegner, D. Mollenhauer, J. Janek and D. Schröder, *Chem. Mater.*, **32**, 3427 (2020).
54. K. Lin, Q. Chen, M. R. Gerhardt, L. Tong, S. B. Kim, L. Eisenach, A. W. Valle, D. Hardee, R. G. Gordon, M. J. Aziz and M. P. Marshak, *Science*, **349**, 1529 (2015).
55. S. Schwan, D. Schröder, H. A. Wegner, J. Janek and D. Mollenhauer, *ChemSusChem*, **13**, 5480 (2020).
56. M. R. Gerhardt, L. Tong, R. Gómez-Bombarelli, Q. Chen, M. P. Marshak, C. J. Galvin, A. A. Aspuru-Guzik, R. G. Gordon and M. J. Aziz, *Adv. Energy Mater.*, **7**, 1601488 (2017).
57. W. Lee, G. Park and Y. Kwon, *Chem. Eng. J.*, **386**, 123985 (2020).
58. W. Lee, A. Permatasari, B. W. Kwon and Y. Kwon, *Chem. Eng. J.*, **358**, 1438 (2019).
59. W. Lee, A. Permatasari and Y. Kwon, *J. Mater. Chem. C*, **8**, 5727 (2020).
60. C. Chu, W. Lee and Y. Kwon, *Korean Chem. Eng. Res.*, **57**, 847 (2019).
61. W. Lee, K. Y. Chung and Y. Kwon, *Korean Chem. Eng. Res.*, **57**, 239 (2019).
62. Y. Lv, C. Han, Y. Zhu, T. Zhang, S. Yao, Z. He, L. Dai and L. Wang, *J. Mater. Sci. Technol.*, **75**, 96 (2021).
63. J. Ryu, M. Park and J. Cho, *J. Electrochem. Soc.*, **163**, A5144 (2015).
64. D. Yang, Y. Guo, H. Tang, Y. Wang, D. Yang, P. Ming, C. Zhang, B. Li and S. Zhu, *Int. J. Hydrogen Energy*, **46**, 33300 (2021).
65. T. J. Carney, S. J. Collins, J. S. Moore and F. R. Brushett, *Chem. Mater.*, **29**, 4801 (2017).
66. S. Kuroda, N. Tobori, M. Sakuraba and Y. Sato, *J. Power Sources*, **119**, 924 (2003).
67. N. Sakai, R. Wang, A. Fujishima, T. Watanabe and K. Hashimoto, *Langmuir*, **14**, 5918 (1998).
68. M. Al-Yasiri and J. Park, *Appl. Energy*, **222**, 530 (2018).